American Mineralogist, Volume 65, pages 885–899, 1980

Solubility mechanisms of carbon dioxide in silicate melts: a Raman spectroscopic study

BJØRN O. MYSEN AND DAVID VIRGO

Geophysical Laboratory, Carnegie Institution of Washington
Washington, D.C. 20008

Abstract

Determinations of carbon dioxide solubility in melts of $CaMgSi_2O_6$ and $NaCaAlSi_2O_7$ composition at high pressure and temperature have been combined with Raman spectroscopic measurements of quenched melts to determine the structural role of CO_2 in silicate melts.

Carbon dioxide solubility increases with increasing temperature under isobaric conditions between 1450° and 1700°C and decreases as a function of increasing temperature below 1450° and above 1700°C. We suggest that these contrasting temperature dependences are a result of similar contrasting behavior of the fugacity of CO_2.

Carbon dioxide dissolves in silicate melts predominantly as CO_3^{2-}. This anion is most likely closely associated with one or more network-modifying cations. In the present melts we suggest that $(CaCO_3)^0$ complexes are formed.

The CO_2 contents of the quenched melts are systematically correlated with structural changes of the network of the melts. The anionic structure of alkaline earth metasilicate melts is predominantly a combination of structural units that, on the average, have 4, 2, and 1 nonbridging oxygens per silicon (NBO/Si). These structures are referred to as monomers, chains, and sheets. The formation of carbonate is associated with a lowering of the proportion of monomers in the melt and an increase of the proportions of chain and sheet units.

The principles of CO_2 solubility mechanisms derived from melt of $CaMgSi_2O_6$ composition also apply to melt of $NaCaAlSi_2O_7$ composition. The solubility mechanisms in the two types of melts differ in detail, however, as the latter melt contains a large proportion of aluminum in tetrahedral coordination, which combined with the silicon results in a higher degree of polymerization of the melt. The $NaCaAlSi_2O_7$ melt consists of structural units that, on the average have 2, 1, and 0 nonbridging oxygens per tetrahedrally coordinated cation (NBO/T). These units are referred to as chains, sheets, and three-dimensional network structures, respectively. When CO_2 is dissolved in such melt, the three-dimensional network units become more dominant at the expense of chain units.

We suggest that the $NaCaAlSi_2O_7$ melt composition is a better model for natural basalt magma than $CaMgSi_2O_6$ melt. On the basis of our observations, we conclude, however, that the predictions of CO_2 solubility behavior in natural basalt melt based on studies with binary silicate systems provide an accurate basis for understanding the role of CO_2 in silicate melts.

Introduction

The presence of CO_2 during the formation and evolution of igneous rocks is well documented. Carbon dioxide is one of the major components of volcanic gases (Gerlach and Nordlie, 1975). It is also a major volatile component in glass and fluid inclusions in phenocrysts in basalts (Roedder, 1965; Green, 1972; Delaney *et al.*, 1978). Its presence in the upper mantle during partial melting is documented (McGetchin and Besancon, 1973; see also Irving and Wyllie, 1975, for review of data).

Phase-equilibrium measurements on CO_2-bearing systems relevant to igneous processes in the upper mantle have shown that the presence of CO_2 results in enhanced stability of more polymerized minerals relative to those observed in the absence of CO_2 (Eggler, 1975; Huang and Wyllie, 1976; Eggler and Rosenhauer, 1978; Eggler *et al.*, 1979). As a result, partial melts of peridotite + CO_2 are more basic than those formed by partial melting of CO_2-free peridotite (Wendlandt and Mysen, 1978).

On the basis of the data summarized above and in-

0003–004X/80/0910–0885$02.00

frared measurements of quenched, CO_2-saturated silicate melts (Mysen *et al.*, 1976; Brey and Green, 1976; Eggler *et al.*, 1979), it has been suggested that CO_2 is dissolved in silicate melts primarily as CO_3^{2-}. It has also been suggested that the silicate melt becomes more polymerized as a result of the formation of this carbonate anion. The effect on the melt structure of solution of CO_2 has not, however, been determined. In order to determine the structural role of CO_2 in rock-forming silicate melts under conditions relevant to magma formation and evolution, Raman spectroscopy of silicate melts with and without CO_2 has been used in conjunction with solubility determinations on selected melt compositions.

Starting materials

Two melt compositions were chosen for CO_2 solubility studies (compositions: $CaMgSi_2O_6$—Di melt, and $NaCaAlSi_2O_7$—Sm melt). In addition, six CO_2-free compositions on the join Ca_2SiO_4–SiO_2 were studied in order to substantiate the band assignments in the CO_2-bearing samples. This join was chosen because of its chemical simplicity; only Si^{4+} is in tetrahedral coordination. The overall ratio of nonbridging oxygens to tetrahedral cation (NBO/T) is a simple function, therefore, of the Ca/Si (atomic) ratio. Furthermore, there are other published data on melt compositions where Ca^{2+} is substituted with other alkaline earth and alkali metal cations.

For the CO_2 solubility studies, Di melt was used, in part because of the significant amount of available experimental data on Di-bearing systems and also because no amphoteric oxides exist in Di melt. A direct correlation between dissolved carbonate anions and their influence on the Si-O network may result. Sm melt was chosen because of the presence of a large proportion of aluminum, which may act as both a network former and a network modifier. In volatile-free Sm melt, all Al is probably a part of the silicate network where Al exist as $(CaAl_2O_4)^0$ or as $(NaAlO_2)^0$ complexes (Virgo *et al.*, 1979). The possibility exists, therefore, that with the formation of CO_3^{2-} anions as $CaCO_3$ or Na_2CO_3 a portion of the aluminate complexes may dissociate, as some of the modifying cations in the aluminate complexes are needed to form carbonate complexes. As a result of this mechanism, some Al may no longer be in the network, and the melt must depolymerize because of dissolved CO_2.

Experimental technique

The starting materials were mixtures of Johnson–Matthey spectroscopically pure SiO_2, Al_2O_3, MgO, and $CaCO_3$, and reagent grade Na_2CO_3. All high-pressure experiments were conducted in solid-media, high-pressure apparatus (Boyd and England, 1960) using sealed Pt containers of 3 mm O.D. in a furnace assembly of 0.5″ diameter. Inasmuch as the furnace parts must be kept dry to avoid formation of H_2 with the resultant formation of reduced carbon species in the experimental charges (Eggler *et al.*, 1974), the furnace parts were dried thoroughly prior to each experiment.

All experiments were carred out with the piston-out technique and with no pressure correction for friction (Boyd and England, 1963). The uncertainty of the pressure is about ±1 kbar. Thermocouples were Pt–Pt90Rh10 with no correction on the electromotive force for pressure. The uncertainty of the temperature due to this simplification is 6°–10°C, depending on the temperature (Mao *et al.*, 1971). Quenching rates were of the order of 250°C/sec.

Selected high-pressure experiments had run durations up to 1 hour at 1700°C. The thermocouple drift at such high temperatures depends, to a large extent, on the purity of the alumina thermocouple insulators (Mao *et al.*, 1971; Presnall *et al.*, 1973). In the present studies, McDanel grade 998 alumina was used in all experiments. With this high-purity alumina, the thermocouple drift is about 10° per hour at 1700°C. Inasmuch as the uncertainty of the temperature is already about 10°C due to the largely unknown influence of pressure of the emf, no further refinement of the temperature monitoring system was carried out.

High-pressure experiments of CO_2-free melts of Di and Sm composition were carried out with glass starting materials. The run durations were the same as for the CO_2-bearing samples at the same temperature and pressure. The one-atm glasses were quenched after 30 minutes at 1500°C. All samples were contained in Pt capsules (sealed).

The six melt compositions on the join Ca_2SiO_4–SiO_2 were prepared at 1650°C in a vertical quench furnace with molybdenum disilicide heating elements. In order to avoid contamination of the samples by conventional quenching in water or mercury, the samples were quenched in a Pt crucible standing in liquid nitrogen. The quenching rate with this technique is on the order of 500°/sec over the first 1000°C.

The CO_2 contents of the quenched melts were measured with beta-track mapping (Mysen and Seitz, 1975), using carbon-14 as source of the beta activity. This activity was recorded on K-5 nuclear emulsions supplied by Ilford Co., England. The stan-

dard was synthetic calcite. The reliability of this method has been tested against determinations by several other techniques (*e.g.*, Kadik and Eggler, 1975; Mysen *et al.*, 1976; Eggler *et al.*, 1979) and is reliable to within less than 5% of the CO_2 content of the sample.

The Raman spectra were taken on small chips of quenched bubble-free melt (about 0.5–1.0 mm cubes). The spectra were recorded with a Jobin-Yvon optical system, holographic grating, double monochromator (HG25), and a photon-counting detection system. The spectra were recorded at 3 cm^{-1}/sec. The samples were excited with the 488.0 mn line of an Ar^+ laser, using a laser power of 200–400 mW at the sample with 90° scattering geometry. Polarized spectra were obtained with the focused exciting beam parallel to the horizontal spectrometer slit and with the electric vector of the exciting radiation in a vertical orientation. A sheet of polarizer disk in front of an optical scrambler was used to record separately the parallel and perpendicular components of the scattered radiation.

As a matter of routine, replicate spectra from the same chips, from different chips of the same experimental run product, and from duplicate experiments were also taken.

Equilibrium considerations

The experiments were routinely conducted with a finely ground oxide + carbonate mixture (1 μm grain size). The carbonate was the source of CO_2. Mysen *et al.* (1976) conducted solubility measurements at fixed pressure and temperature but with run durations varying from 1 to 60 min. They found that in a viscous melt such as that of $NaAlSi_3O_8$ composition, less than 5 min was needed to reach equilibrium CO_2 concentrations at 1450°C and 20 kbar. Longer run durations did not affect the results. In the present study experiments of 5 min or longer were always used. In addition, reversal experiments at 20 kbar and 1685°C were carried out. These conditions were chosen because the forward experiments indicated that melts quenched from this temperature and pressure contained the largest amount of CO_2. In the reversal experiments the sample was first subjected to 10 kbar and 1650°C for 10 min, where the forward experiments indicated that the solubility was less than 50 percent of that at 20 kbar and 1685°C. The conditions were then changed to 20 kbar and 1685°C. About 60 min under these conditions was needed to reach the same CO_2 concentrations as in the initial experiment. Shorter run durations resulted in heterogeneous charges. The much longer run lengths needed to achieve equilibrium in the reversal experiments can be understood by considering the diffusion distances of CO_2 in the two types of experiment. During a forward experiment, CO_2 needs to move only a few micrometers to become thoroughly mixed with the oxide components because of the fine-grained, thoroughly mixed nature of the starting material. The CO_2 that does not dissolve in the melt enters a separate vapor phase. During a reversal experiments some of the CO_2 that initally entered the vapor phase must redissolve in the melt and move perhaps several hundred micrometers into the liquids, thus requiring longer time for equilibration.

This agreement between the forward and reversal experiments indicates that the run durations used for the routine experiments were sufficient to attain equilibrium CO_2 contents of the melts.

Results

CO_2 solubility

The carbon dioxide solubilities in the melts and other experimental details are shown in Table 1. The reversal experiment is marked with an asterisk. Carbon dioxide contents of quenched melts of Di composition as a function of temperature and pressure are shown in Figure 1. The solubilities agree with those of Mysen *et al.* (1976) in the pressure and temperature ranges also studied by them. Whereas Mysen *et al.* (1976) suggested essentially no temperature dependence of the solubility at 10 kbar, the present data may indicate a very slight decrease in CO_2 content with increasing temperature above 1600°C at this pressure. At 20 kbar the CO_2 solubility in Di melt increases rapidly from 1580° to about

Table 1. Run data

Sample No.	Composition	Pressure, kbar	Temp., °C	Run Duration, min	Wt % CO_2
997	Di + CO_2	10	1550	10	1.55 ± 0.02
1014	Di + CO_2	10	1600	10	2.00 ± 0.06
995	Di + CO_2	10	1650	10	1.95 ± 0.05
1018	Di + CO_2	10	1725	5	1.85 ± 0.07
1036	Di + CO_2	20	1580	15	3.1 ± 0.1
1000	Di + CO_2	20	1650	5	3.38 ± 0.08
1023	Di + CO_2	20	1685	5	4.8 ± 0.2
1002	Di + CO_2	20	1725	5	2.71 ± 0.09
1004	Di + CO_2	25	1725	5	3.6 ± 0.1
1039*	Di + CO_2	20	1685	60	5.0 ± 0.2
1056	Sm + CO_2	10	1275	60	5.2 ± 0.2
1073	Sm + CO_2	10	1460	15	3.9 ± 0.2
1074	Sm + CO_2	10	1550	10	3.8 ± 0.1
1062	Sm + CO_2	20	1325	30	4.9 ± 0.2
1068	Sm + CO_2	20	1460	15	4.4 ± 0.2
1072	Sm + CO_2	20	1550	10	5.9 ± 0.3

*Reversal.

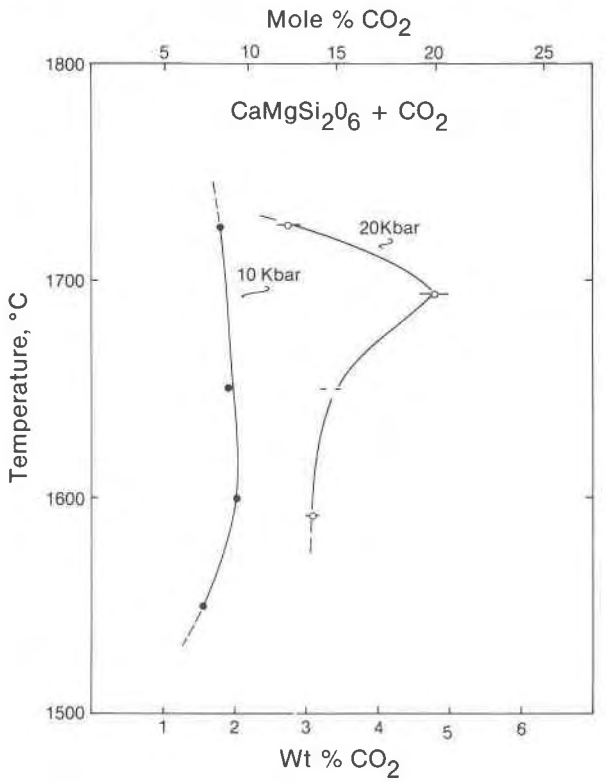

Fig. 1. Carbon dioxide solubility in Di melt as a function of temperature and pressure.

1700°C. As the temperature is raised further, the CO_2 content of the melt is lowered. There is therefore a maximum of the CO_2-solubility curve for Di melt at 20 kbar. The CO_2 solubility at 1685°C and 20 kbar was confirmed by replicate experiments, time studies, and reversal experiments. This maximum CO_2 solubility was not observed by Mysen *et al.* (1976) because they did not extend their experiments to sufficiently high temperatures. Holloway *et al.* (1976) found, however, that CO_2 solubilities in melts on the join Ca_2SiO_4–Mg_2SiO_4 also reached a maximum and then decreased as the temperature was raised above 1700°C at 20 kbar, and they suggested a structural interpretation for this observation. The CO_2 solubility in a melt of natural nephelinite composition (Mysen *et al.*, 1975) also passed through a maximum near 1700°C at 20 kbar (Mysen and Eggler, unpublished data, 1977).

Inasmuch as the structures of ortho- and metasilicate melts differ substantially in the degree of polymerization (Brawer and White, 1975; Verweij and Konijnendijk, 1976; Furukawa *et al.*, 1978), it is not likely that the hypothesis of Holloway *et al.* (1976), suggesting that the melt must be nearly completely depolymerized at 1700°C, can be used to explain the data.

The carbon dioxide solubility in Sm melt displays a more complex behavior with temperature than is the case for Di melt (Figs. 1 and 2). At both 10 and 20 kbar the solubility decreases with increasing temperature immediately above the liquidus (above about 1300°C). At 10 kbar the rate of decrease diminishes as the temperature is increased, whereas at 20 kbar the CO_2 solubility in Sm melt passes through a minimum with increasing temperature at about 1450°C. At high temperature the CO_2 solubility increases.

Data on carbon dioxide solubility in silicate melts at temperatures below 1460°C are scarce. It is not possible to decide, therefore, whether the unusual temperature dependence of the solubility in the temperature range below 1450°C in Sm melt is due to the thermodynamic properties of CO_2 or to the structural features of Sm melt in this temperature range.

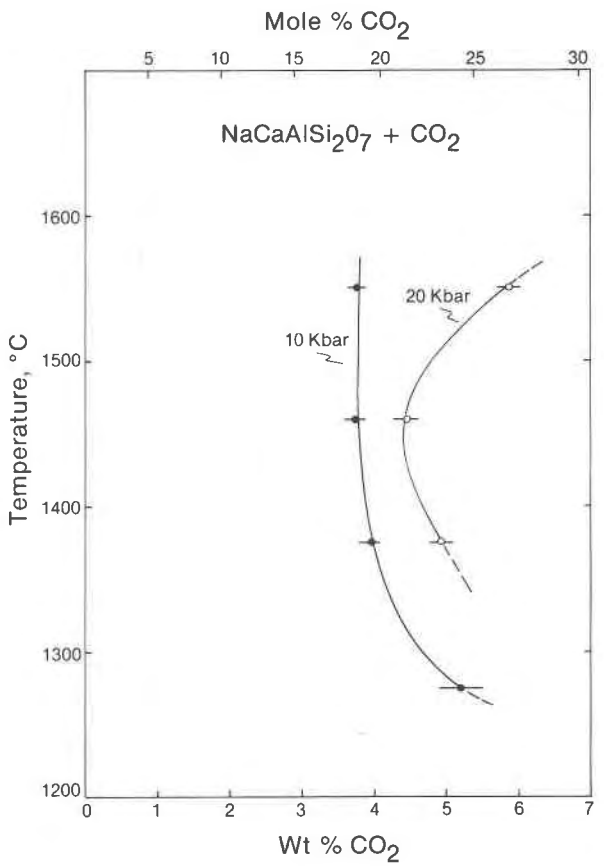

Fig. 2. Carbon dioxide solubility in Sm melt as a function of temperature and pressure.

Raman spectroscopy

In order to provide a framework for Raman spectroscopic band assignments, Virgo *et al.* (1980) acquired spectra of 14 quenched melts on the joins Ca_2SiO_4–SiO_2 and $CaMgSiO_4$–SiO_2. These spectra were also compared with the published data on the joins Li_2O–SiO_2, Na_2O–SiO_2, K_2O–SiO_2, CaO–SiO_2, and PbO–SiO_2 (Brawer and White, 1975, 1977; Verweij and Konijnendijk, 1976; Verweij, 1979a,b; Furukawa *et al.*, 1978; Furukawa and White, 1980). A result of this comparative study was that for all these compositions, at given metal cation to silicon ratio, the same Raman bands occur. The spectra differ somewhat in resolution, however, presumably because of variations in local disorder (Brawer, 1975).

The spectra with the best resolution of important stretch bands are found on the join Ca_2SiO_4–SiO_2 (Fig. 3; see also Table 2). The dominant feature of each spectrum is the intense, slightly asymmetric band in the region 610–673 cm^{-1} combined with an intense, high-frequency envelope in the region 830–1060 cm^{-1}. All these bands are strongly polarized. The Raman spectra on the join $CaMgSiO_4$–SiO_2 are similar to those of analogous melts along the join Ca_2SiO_4–SiO_2 (Virgo *et al.*, 1980).

On the basis of comparison with appropriate crystalline analogues, and experimental and theoretical considerations (Lazarev, 1972; Etchepare, 1972; Brawer, 1975; Brawer and White, 1975, 1977; Furukawa *et al.*, 1978; Furukawa and White, 1980; Verweij, 1979a,b; Sharma *et al.*, 1979; Virgo *et al.*, 1980), we conclude that the band assignments summarized in Table 3 represent the best interpretation of the Raman data summarized above and exemplified with Figure 3 and Table 2.

The most important observation made from the above assignment of the Raman spectra is that there is a unique set of coexisting anionic structural units for specific ranges of the ratio of nonbridging oxygen to silicon. In Table 3, the anionic units are defined on the basis of average NBO/Si. There are several aspects of these conclusions that warrant further comment. In comparison to other models of melt structure (*e.g.*, Masson, 1968), the present model is strikingly simple. This simplicity should not be surprising in view of the fact that when comparing the crystal structures of silicate minerals, only a few anionic structural arrangements can be found (see Dent Glasser, 1979, for review).

Previous models of silicate melt structures involve features such as trimers, tetramers, pentamers *etc.* in addition to rings and branched chains. The experimental basis for most of those models has been chromatographic data derived from trimethylsilyl derivatives of the silicate polymers (TMS derivatives). When applying that method to glass structural determinations, certain apparent inconsistencies appear. First, when comparing results from TMS-derivative studies to structural data derived from Raman spectroscopy of the same materials, the results differ (compare, for example, the results of Lentz, 1964

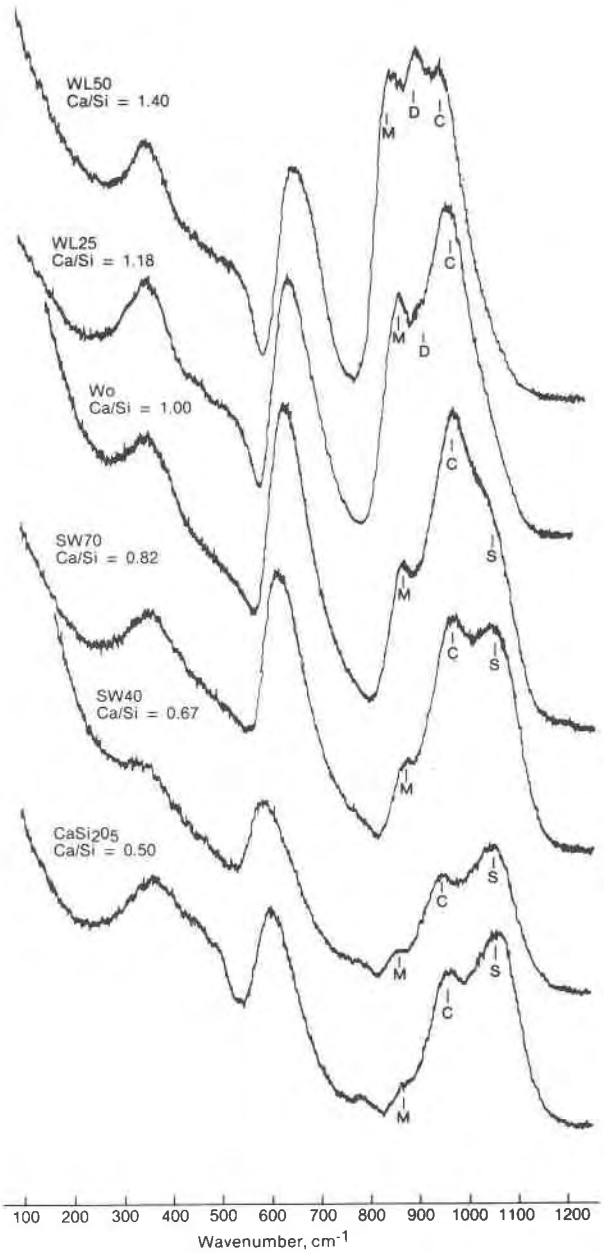

Fig. 3. Unpolarized Raman spectra of quenched melts on the join Ca_2SiO_4–SiO_2. All samples were quenched from 1650°C at 1 atm pressure after 30 minutes. (Ar^+ laser, 200–400 mW power.)

Table 2. Raman data on quenched melts in the system Ca_2SiO_4–SiO_2

Composition	Wavenumber, cm^{-1}						
WL 50	352m,p	547(Sh)	670s,p	830s,p	900s,p	960s,p	...
WL 25	350s,p	547(Sh)	647s,p	853s,p	927m,p	970s,p	...
Wo	345m,p(bd)	...	620s,p	867s,p	...	962s,p	1050m,p
SW 70	343w(bd)	...	613s,p	869w,p	...	963s,p	1051s,p
SW 40	341w(bd)	...	586s,p	863vw	...	957s,p	1055s,p
$CaSi_2O_5$	355m(bd)	...	593s,p	861vw	...	958s,p	1057s,p

Symbols: *WL 50, Ca/Si = 1.40; WL 25, Ca/Si = 1.18; Wo, Ca/Si = 1.00; SW 70, Ca/Si = 0.82; SW 40, Ca/Si = 0.67 $CaSi_2O_5$, Ca/Si = 0.50. All ratios are atomic ratios.*

vw, very weak; w, weak; m, medium; s, strong; (bd), broad; (Sh), shoulder; p, polarized Uncertainty on each measurement is about ± 5 cm^{-1} except for (Sh) where the uncertainty is near 15 cm^{-1}.

with Brawer and White, 1975 for the system Na_2O–SiO_2, and the data of Smart and Glasser, 1979 with those of Furukawa *et al.*, 1978 for the system PbO–SiO_2). Second, results obtained with the TMS derivatives are internally inconsistent. For compositions Pb_2SiO_4 and Na_4SiO_4, the melts have NBO/Si = 4. The results from the work with TMS derivatives indicate that NBO/Si is less than 3 (Smart and Glasser, 1979; Lentz, 1964). We suggest that the reason for this discrepancy is condensation of silicate polymers taking place during solution of the glasses in acid solutions to form the TMS derivatives.

Another feature of most models of melt structure is a positive correlation between order and proportion of silicate polymers and bulk NBO/Si of the melt. In Raman spectroscopic studies, such an evolution would result in a successive increase of the frequency of Si–O stretch bands as the number of Si^{4+} cations in the polymers increases (*e.g.*, Lazarev, 1972; Brawer and White, 1975; Furukawa and White, 1980; see also Table 3). On this basis it would be expected that if anionic structural units with degree of polymerization between dimers and chains were formed on the various binary silicate joins indicated above (see also Fig. 3), new bands would develop or bands such as that near 900 cm^{-1} (Fig. 3; Table 2) would shift to higher frequency as the M/Si of the melt decreased. There is no spectroscopic evidence for such developments. We conclude, therefore, that structural units with NBO/Si between that of a dimer and that of a chain do not exist in significant amounts in silicate melts.

The structural unit with NBO/Si = 2 has been referred to as a chain structure. Ring structures have, however, the same NBO/Si. The idea of the presence of ring structures in silicate melts has experimental support in studies of TMS derivatives of silicate melts (*e.g.*, Masson, 1968). In view of the discussion above, it is not clear whether such data give an accurate description of the structure of the melt itself. Spectroscopic data relevant to the formation of ring structures are scarce. Lazarev (1972) discussed spectroscopic imprints of ring structures with up to 6 silicons. The simple $Si_3O_9^{6-}$ ring has a strong deformation band near 750 cm^{-1}. No such band occurs in the spectra discussed here and elsewhere. This type of a

Table 3. Raman frequencies of the stretch vibrations of specific Si-rich anionic units in silicate melts

Structural unit	NBO/Si	Frequency (cm^{-1})	Characteristics of vibrational mode
SiO_4^{4-}	4	850–880	symmetric stretch
$Si_2O_7^{6-}$	3	900–930	symmetric stretch
$Si_2O_6^{4-}$	2	950–970	symmetric stretch
$Si_2O_5^{2-}$	1	1050–1100	symmetric stretch
SiO_2	0	1065–1200	antisymmetric stretch

Data from Virgo et al. (1980). See text for further discussion.

ring probably does not occur in these melts, therefore. Larger rings (*e.g.*, $Si_4O_{12}^{8-}$–$Si_6O_{18}^{12-}$) show vibrational bands at or slightly above 1100 cm^{-1} (Lazarev, 1972). On a spectroscopic basis alone it is not likely, but not impossible, that the S-band indicated in Figure 3 is such a band, as its frequency is near 1070 cm^{-1}. Furthermore, mass balance considerations indicate that the Raman band in this spectroscopic region reflects vibrations in structural units with NBO/Si less than 2. Consider, for example, the spectrum Wo ($CaSiO_3$) in Figure 3. The Wo composition has bulk NBO/Si = 2. The strong 870 cm^{-1} and an even stronger 970 cm^{-1} band reflect the presence in the melt of structural units with NBO/Si = 4 and 2, respectively. In order to maintain mass balance of oxygen and silicon, there must be structural units in this melt that have NBO/Si less than 2. Careful analysis by in particular Verweij (1979a,b) and Furukawa and White (1980) and also by Virgo *et al.* (1980) has led to the conclusion that the band in the frequency range between 1070 and 1100 cm^{-1} in the MO–SiO_2 and M_2O–SiO_2 melts most likely is a stretch vibration from a unit that has NBO/Si = 1. One might suggest that such a vibrational mode could stem from end units in a linear structure. Such an interpretation does not, however, provide for structural units that satisfy the mass balance of the melt. It might also be suggested that the presence of branched chains or multiple chains in the melt constitutes the structural unit(s) with NBO/Si less than 2. The end result of the evolution of such branching is, of course, an infinite sheet. The frequency of the band in question (denoted S in Fig. 3) does not shift with changes in M/Si. Its intensity increases with decreasing M/Si, however. On this basis, we conclude that the NBO/Si of this structural unit does not vary with changes of bulk NBO/Si of the melt. The possibility of a branched chain is considered unlikely for two reasons. First, there is no experimental evidence for the presence of such structures in silicate melts (branched chains with NBO/Si less than 2). Second, according to a survey by Dent Glasser (1979), branched chains do not occur in minerals. Instead, chains or sheets are formed. There is no clear reason, therefore, why one would expect such a structure in a melt.

A possible explanation for the 1070 cm^{-1} band is multiple chains. The Raman data do not establish whether the S-band (Fig. 3) is an infinite sheet or a finite sheet (multiple chains). In view of the data summarized above, the structural unit probably has an average NBO/Si near 1 (infinite sheet), and the structural units represented by this Si–O stretch band in the Raman spectra will be referred to as a sheet.

Because the relative integrated intensities of the bands assigned to the different anionic species may not be linearly related to NBO/Si, only a general discussion of their relative abundances in these silicate melts is possible at this time. We suggest that monomers are the most abundant species in the melts near the orthosilicate composition and that they become increasingly unstable with increasing NBO/Si, but are still present in the $CaSi_2O_5$ sheet composition. In contrast, the dimer unit has a restricted range of stability, with an apparent maximum in its abundance between the ortho- and metasilicate compositions. The instability of the dimer species appears to coincide with the appearance of the sheet unit, and with increasing NBO/Si the sheet and chain species increase in abundance relative to the monomer units.

In view of the above results and mass-balance considerations, we propose that the equilibria relating the coexisting anionic species are the following disproportionation reactions, which correspond to the specific ranges of NBO/Si indicated above:

$$2Si_2O_7^{6-} = 2SiO_4^{4-} + Si_2O_6^{4-} \quad (1)$$

and

$$3Si_2O_6^{4-} = 2SiO_4^{4-} + 2Si_2O_5^{2-} \quad (2)$$

$CaMgSi_2O_6 + CO_2$

Raman spectra of volatile-free Di melt at several temperatures and pressures are shown in Figure 4, and band assignments are given in Table 4. The spectra show an overall similarity in that the same bands occur at all temperatures and pressures. All bands are polarized.

The spectra of quenched Di melt consist of a broad envelope between 850 and 1105 cm^{-1}, containing at least three bands. The strongest band is at 970–980 cm^{-1} and does not change frequency appreciably with changing temperature or pressure. A higher-frequency band of strong intensity occurs as a shoulder near 1050 cm^{-1}. A third band of intermediate intensity is between 860 and 880 cm^{-1}. This band occurs as a shoulder under all conditions. In addition to the high-frequency envelope, there is a strong band near 640 cm^{-1} that shifts to slightly lower frequency with decreasing temperature. The spectra closely resemble that of Wo melt in Figure 3.

Three bands of Gaussian form were fitted inside the high-frequency envelope of the spectra shown in Figure 4. Although the presence of more than three

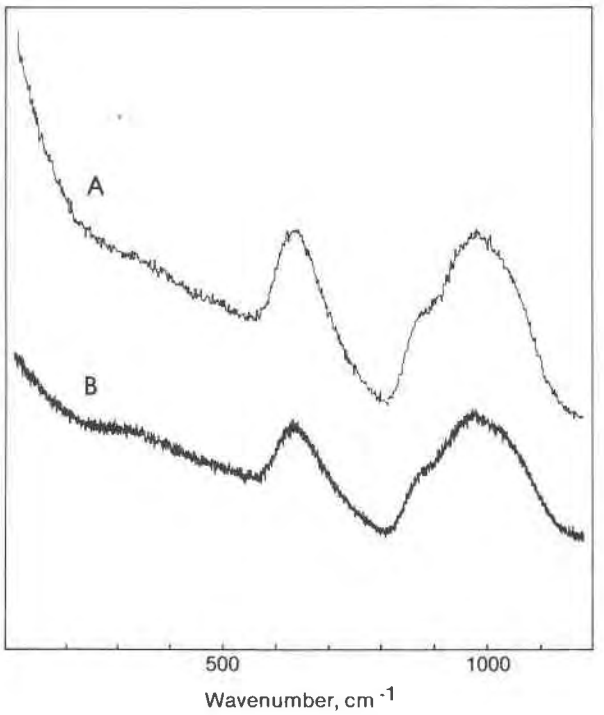

Fig. 4A. Unpolarized Raman spectra of quenched Di melt at 1 atm and 1550°C (*A*) and 1400°C (*B*). (Ar^+ laser, 200–400 mW power.)

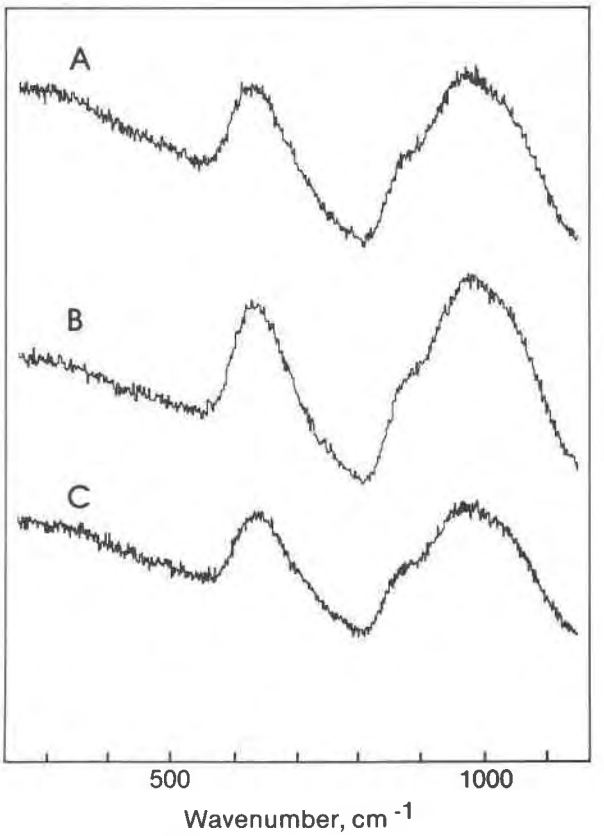

Fig. 4B. Unpolarized Raman spectra of quenched Di melt at 10 kbar and 1550°C (*A*), 10 kbar and 1650°C (*B*), and 20 kbar and 1685°C (*C*). (Ar^+ ion laser, 4880 A line, 200–400 mW power.)

bands cannot be ruled out, the spectra shown here (Figs. 3 and 4), as well as data from other relevant systems discussed or referred to above, indicate that only three bands are present. When the data were fitted, the maximum of the high-frequency envelope was initially assumed to coincide with the maximum of the strongest band, and the lower portion of the low-frequency limb of the high-frequency envelope was set to coincide with the low-frequency limb of a band near 870 cm^{-1} (its presence is indicated by the shoulder in Fig. 4). The cumulative area of the three bands thus fitted within the high-frequency envelope equals the area of the envelope within the statistical uncertainty of the spectra themselves. The results of this fitting procedure for quenched Di melts as a function of pressure and temperature are shown in Figure 5. The frequencies of all bands are independent of pressure and temperature. It should be emphasized that the existence and frequency of the stretch bands in the high-frequency envelope are also evident from the raw Raman data. The curve fitting was carried out simply in an attempt to get a better impression of the intensity ratios and a more accurate determination of the frequencies of the individual bands. Consequently, the structural interpretation of the Raman spectra insofar as the individual structural units are concerned is not affected by the curve-fitting procedure. The procedure will, however, give an impression about how the proportions of the individual structural units vary.

The Raman spectra of quenched Di melt indicate, therefore, that such melts consist of anionic structural units with an average of 4, 2, and 1 NBO/Si. The equilibrium between these units may be expressed with equation 2 above. The proportions of the units in a quenched melt are related to the relative intensities of the bands at 870 cm^{-1} (monomer), 970 cm^{-1} (chain), and 1070 cm^{-1} (sheet). As a melt becomes more disproportioned, the intensity ratios $I(970)/I(870)$ and $I(970)/I(1070)$ will decrease. The rate of change of these intensity ratios is not linearly related to molar proportions of the structural units, however, because the molar scattering coefficients differ for the different vibrations considered. The intensity ratios are listed in Table 4. These data show that both intensity ratios decrease with decreasing

Table 4. Raman spectroscopic data, $CaMgSi_2O_6 + CO_2$

Sample No.	Composition	P, kbar	T, °C	Wavenumber, cm^{-1}								$\frac{I(970)}{I(870)}$	$\frac{I(970)}{I(1070)}$
1007	Di	0.001	1585	...	632s,p	880m,p	983s,p	1070m,p	...	...	...	...	3.57	2.53
1006	Di	0.001	1425	...	633s,p	880m,p(sh)	980s,p	1068m,p(sh)	...	...	...	...	5.33	5.61
1013	Di	10	1650	...	629s,p	873m,p(sh)	975s,p	1070m,p(sh)	...	...	...	...	3.70	2.36
1017	Di	20	1650	...	629s,p	873m,p(sh)	975s,p	1070m,p	...	...	...	...	5.63	4.59
1024	Di	20	1685	...	636s,p	872m,p(sh)	978s,p	1066m,p	...	...	...	...	3.55	2.66
997	Di + CO_2	10	1550	...	630s,p	874m,p	965s,p	1040m,p	1075s,p	...*	...*	...*	...	...
1014	Di + CO_2	10	1600	...	630s,p	873m,p	970s,p	1035m,p	1075s,p	...*	...*	...*	...	...
995	Di + CO_2	10	1650	...	630s,p	874m,p	963s,p	1035m,p	1078s,p	...*	...*	...*	3.72	3.29
1000	Di + CO_2	20	1650	...	628s,p	862m,p(sh)	965s,p	1038w,p	1073s,p	...*	...*	...*	5.55	5.05
1023	Di + CO_2	20	1685	467m,p(sh)	605s,p	863vw,p(sh)	963s,p	1023w,p	1070s,p	1420vw,p	1525vw,p	1730vw,p	17.0	17.0
1002	Di + CO_2	20	1725	...	624s,p	865m,p	964s,p	1030w,p	1073s,p	...*	...*	...*	4.59	5.39
1004	Di + CO_2	25	1725	...	610s,p	879w,p	964s,p	1040w,p	1073s,p	...*	...*	...*	5.75	3.64

*Band present, but too weak for assignment.
Uncertainty ± 5 cm^{-1}.
Symbols: s, strong; m, medium; w, weak; vw, very weak; p, polarized; (sh), shoulder.

temperature under isobaric conditions and with decreasing pressure under isothermal conditions. The temperature effect is greater at 20 kbar than at 1 atm, because the percentage change of both intensity ratios is similar between 1425° and 1585°C at 1 atm and between 1650° and 1685°C at 20 kbar. The proportion of chain relative to monomer and sheet decreases by about the same amount between 20 and 10 kbar at 1650°C as between 1650° and 1685°C at 20 kbar for quenched, volatile-free Di melt (Table 4).

Addition of CO_2 to quenched Di melt results in new bands at 1080, 1450, 1525, and 1730 cm^{-1} (see Fig. 6 and Table 4). Furthermore, the 650 cm^{-1} band has developed an asymmetry toward higher frequency. This asymmetry may be caused by another unresolved band near 700 cm^{-1}. These bands are characteristic of the carbonate ion (White, 1974; Verweij *et al.*, 1977), the only difference being two bands at 1450 and 1525 cm^{-1} rather than one or only a minor splitting into two. This large band separation (75 cm^{-1}) may be due to deformation of the CO_3^{2-} anionic complex relative to the highly symmetric CO_3^{2-}

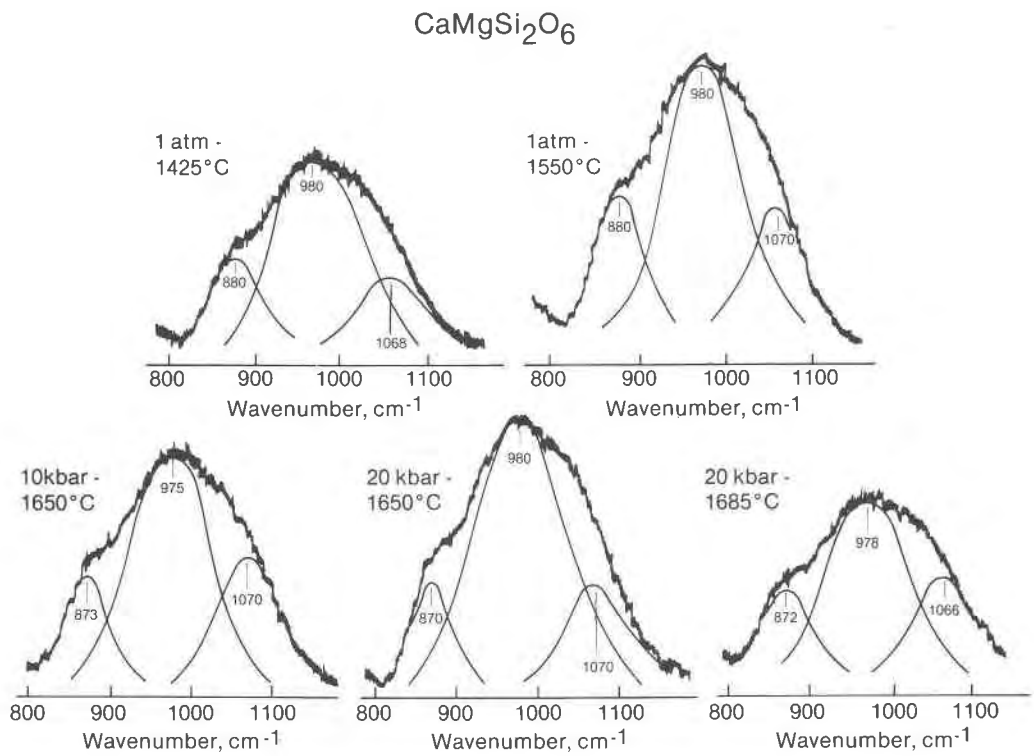

Fig. 5. Results of fitted lines inside the high-frequency envelope of Raman spectra of quenched Di melt as a function of temperature and pressure (see text for procedure).

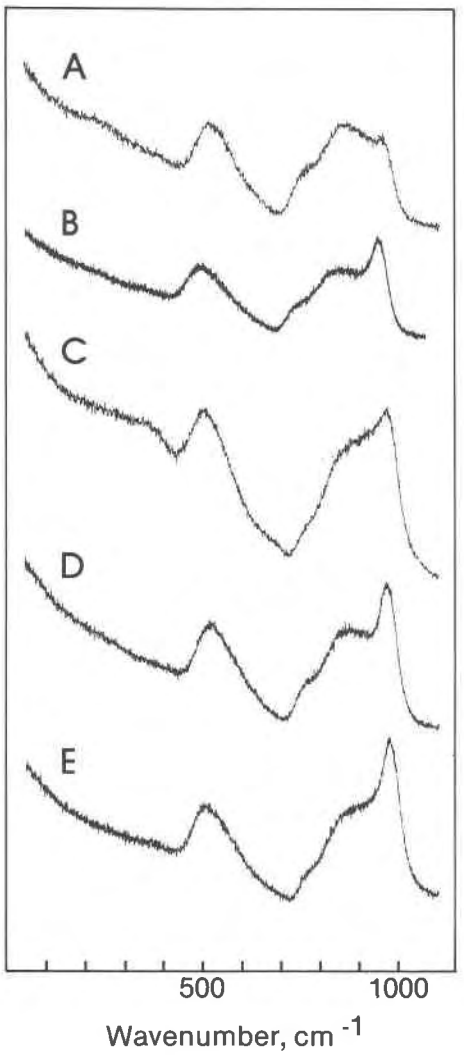

Fig. 6. Unpolarized Raman spectra of Di + CO_2 melts at 10 kbar and 1650°C (*A*), 20 kbar and 1650° (*B*), 20 kbar and 1685°C (*C*), 20 kbar and 1725°C (*D*), and 25 kbar and 1725°C (*E*). (Ar^+ ion laser, 4880 A line with 200–400 mW power.)

found in crystalline $CaCO_3$, for example. There is no evidence in the Raman spectra to indicate the reason for such deformation.

The spectra reflecting the silicate anionic network of CO_2-saturated, quenched Di melts resemble those of CO_2-free melts (Figs. 4–6). There are, however, systematic shifts of frequencies and intensity ratios as a function of CO_3^{2-} of the quenched melts.

At 10 kbar the CO_2 solubility is about 2 wt. percent (9 mole percent CO_3^{2-}), with only minor temperature dependence. The 630 cm^{-1} band (Si–O^0 bending characteristic of $Si_2O_6^{4-}$ chains) remains near 630 cm^{-1} at 10 kbar pressure. In the high-frequency envelope three bands near 880, 970, and 1070 cm^{-1} can be discerned in the raw Raman data (Fig. 6). The 1070 cm^{-1} C–O stretch band occurs at nearly the same frequency as the stretch band indicative of sheet structural units in the CO_2-free melt (Tables 2–4). This is also the frequency region where antisymmetric stretch bands from structural units with NBO/Si = 0 are anticipated (Table 3). A three-dimensional array of SiO_4 tetrahedra also results in two deformation bands between 430 and 480 cm^{-1} (*e.g.*, Bates *et al.*, 1974). Such bands do not occur in the present spectra (Fig. 6; see also Table 4). We conclude, therefore, that three-dimensional network units do not occur in Di melt with several wt. percent CO_2 in solution. In view of the overall similarity of the Raman spectra resulting from vibrations in silicate tetrahedral complexes, it seems reasonable to assume that there is another Raman band near (perhaps at the same frequency as) the C–O stretch band at 1070 cm^{-1}.

The data in Figure 6 (see also Tables 1 and 4) show that as the CO_2 content of the Di melt increases, the intensity of the band near 870 cm^{-1} decreases. Consequently, we conclude that the proportion of monomers in the melt structure decreases relative to the other structural units as the CO_2 content of the melt increases.

As the CO_2 content of the melt is increased, the frequency of the band near 650 cm^{-1} shifts toward 600 cm^{-1}. This observation is interpreted to mean that the proportion of structural units with NBO/Si less than 2 becomes more important relative to other structural units as the CO_2 content of the melt is increased.

$NaCaAlSi_2O_7 + CO_2$

Provided that Al is in tetrahedral coordination in Sm melt, this melt has the same number of nonbridging oxygens per tetrahedrally coordinated oxygen as sodium trisilicate melt ($Na_2Si_3O_7$). According to available data (*e.g.*, Taylor and Brown, 1979, Virgo *et al.*, 1979), Al is tetrahedrally coordinated in silicate melts provided that sufficient metal cations are present to maintain a local charge of 4+ near the tetrahedral cation. This requirement will be referred to as local charge balance.

It has been shown (*e.g.*, Virgo *et al.*, 1979) that tetrahedrally coordinated Al in a given structural unit results in a downward shift of the frequency of the associated stretch band that is positively correlated with the Si/(Si + Al) of the structural unit under consideration. In addition to this effect, such Si(Al) coupling results in loss of spectroscopic resolution,

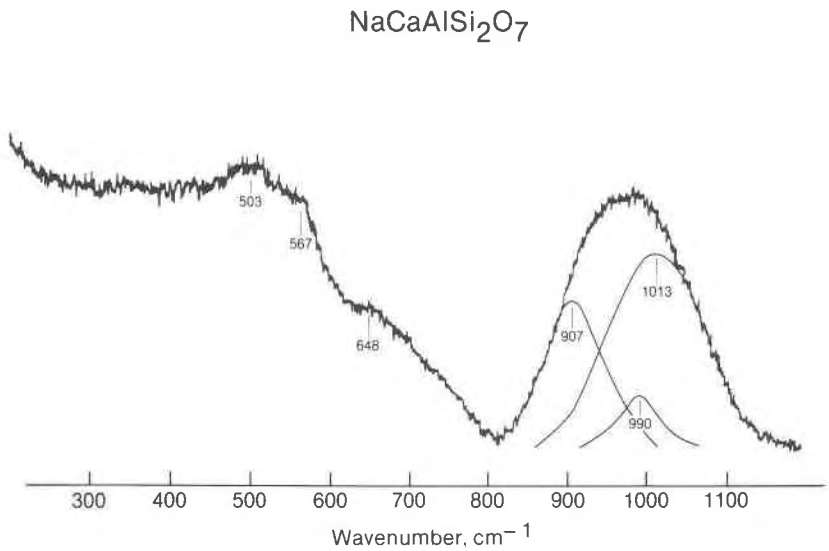

Fig. 7. Unpolarized Raman spectrum of volatile-free Sm melt at 10 kbar and 1275°C. See text for discussion of suggested line-fitting in the high-frequency envelope. (Ar^+ laser, 200–400 mW power.)

probably because of increased local disorder. Consequently, the interpretation of the Raman spectra of Sm melt (19.74 wt. percent Al_2O_3) is difficult. In view of the similar stoichiometry of $Na_2Si_3O_7$ and Sm melt compositions, published Raman spectroscopic results from the former composition (Furukawa and White, 1979) will be used as an aid in interpreting the Sm spectra. Furukawa and White (1980), in a careful analysis of the band assignments in the Raman spectrum of $Na_2Si_3O_7$ melt, concluded that the sheet unit was the major structural unit in the melt. In addition, there is a band near 950 cm^{-1} which is assigned to a structural unit with NBO/Si = 2 (chain). From a mass-balance point of view, quenched melt of $Na_2Si_3O_7$ composition (NBO/Si = 0.67) must also contain at least one structural unit with NBO/Si considerably less than 1. Virgo *et al.* (1980) found evidence for this unit in the existence of rocking bands near 650 cm^{-1} and a bending band near 800 cm^{-1}. These frequencies correspond to those found for three-dimensional structural units. The associated Si–O stretch band most likely occurs near 1060 cm^{-1}. Its spectroscopic signature is, however, probably obliterated by the intense 1100 cm^{-1} band in this composition.

The Raman spectrum of Sm melt is shown in Figure 7 (see also Table 5). The band near 500 cm^{-1} is near the same frequency as the (Si,Al)–O^0 rocking (deformation) band observed in melts with a three-dimensional network structure on the joins $CaAl_2O_4$–SiO_2 and $NaAlO_2$–SiO_2 (Brawer and White, 1977; Virgo *et al.*, 1979), and is considered characteristic of melts with a three-dimensional network unit. The band near 650 cm^{-1} is assigned to (Si,Al)–O^0 bending and at this frequency is characteristic of a chain unit (see also above).

The high-frequency envelope is asymmetric and indicates the presence of at least two bands. This fre-

Table 5. Raman spectroscopic data, $NaCaAlSi_2O_7 + CO_2$

Sample No.	Composition	P, kbar	T, °C	Wavenumber, cm^{-1}									
1059	Sm	0.001	1460	...	493m,p	560m,p	651m,p	...	...	900w,p(sh)	980s,p	...	...	...	...
1057	Sm	10	1275	...	500m,p	553m,p	662m,p	...	...	900w,p(sh)	980s,p	...	...	...	...
1056	Sm + CO_2	10	1275	...	493s,p	566m,p	683m,p†	716w,p	860w,p(sh)	942s,p	1000s,p	1070s,p	1413vw,p	1513vw,p	1737vw
1073	Sm + CO_2	10	1460	...	497s,p	557m,p	670m,p†	707w,p(sh)	860w,p(sh)	930s,p(sh)	993s,p	1070s,p	...*	...*	...*
1074	Sm + CO_2	10	1550	...	490s,p	557m,p	650w,p	683w,p	860vw,p(sh)	922m,p	990s,p	1070s,p	...*	...*	...*
1062	Sm + CO_2	20	1325	279m	482s,p	550m,p(sh)	...	700m,p	860vw,p(sh)	942s,p	997s,p	1075s,p	n.m.	n.m.	n.m.
1068	Sm + CO_2	20	1460	...	493s,p	560m,p	627vw,p	700m,p	860vw,p(sh)	940s,p	1006s,p	1075s,p	n.m.	n.m.	n.m.
1072	Sm + CO_2	20	1550	...	490s,p	560m,p	...	707m,p	860w,p(sh)	950s,p	1010s,p	1070s,p	n.m.	n.m.	n.m.

*Band present, but too weak for assignment.
†Broad.
Uncertainty ±5 cm^{-1}.
Symbols: n.m., not measured; others as in Table 2.

quency region differs considerably from that obtained for crystalline $NaCaAlSi_2O_7$ (Sharma, 1979) where the major band is very near 900 cm^{-1} (Si_2O_7 dimer in crystalline material). In analogy with the conclusions for quenched $Na_2Si_3O_7$ melt, the main band in the high-frequency envelope should stem from stretch vibrations in a structural unit with an average NBO/T = 1. The above interpretations, which are independent of the data contained in the high-frequency envelope, indicate that three-dimensional structural units as well as units with NBO/T = 2 also occur in this melt. These conclusions imply that at least three stretch bands must be located in the high-frequency envelope. Curve-fitting involving unresolved bands should be carried out with great caution, and the curves inserted in the high-frequency envelope in Figure 7 should only be considered as a suggestion. In deriving this suggested solution it was assumed that Al was randomly distributed between the three structural units and that the influence of Si(Al) coupling on the frequencies of the relevant stretch bands is relatively similar. A consequence of this assumption is that all the stretch bands should be at a lower frequency than the analogous bands in the Al-free $Na_2Si_3O_7$ melt composition. If the calibration of Virgo *et al.* (1979) for frequency shift of antisymmetric stretch bands in three-dimensional network structures on the joins $NaAlO_2$–SiO_2 and $CaAl_2O_4$–SiO_2 as a function of Si/(Si + Al) were used, each stretch band in the Sm melt composition would shift by approximately 70 cm^{-1} relative to their positions in $Na_2Si_3O_7$. Finally, the location of the two shoulders on the high-frequency envelope were taken as an indication of approximate position of the two strongest bands in the envelope, and the form of the high- and low-frequency limbs of the envelope was used as a guide for the form of the high- and low-frequency limbs of these two bands. With all these considerations in mind, the curve-fitting shown in Figure 7 was produced. With this interpretation, the strong 1013 cm^{-1} band is an Si(Al)-coupled stretch band from a structural unit with, on the average, NBO/T = 1. The 990 cm^{-1} band stems from a three-dimensional structural unit and the 907 cm^{-1} band from a structural unit with about 2 nonbridging oxygens per tetrahedrally coordinated cation.

The three structural units are denoted T_2O_6, T_2O_5, and TO_2, where T = Si + (NaAl) + (1/2$CaAl_2$). The equilibrium between the three structural units may be expressed with the equation

$$2T_2O_5^{2-}\ (\text{sheet}) = T_2O_6^{4-}\ (\text{chain}) + 2TO_2\ (3D) \quad (3)$$

Addition of carbon dioxide to Sm melt results in the appearance of the characteristic carbonate bands (1070, 1420, 1520, and 1740 cm^{-1}; White, 1974) seen in Figure 7 (see also Table 5). In addition to these bands, a weak band occurs near 700 cm^{-1}. This band is characteristic of the in-plane deformation mode of the CO_3^{2-} anion (Verweij *et al.*, 1977; White, 1974). It cannot be observed in CO_2-bearing Di melt (Fig. 5) because it lies beneath the high-frequency limb of the strong Si–O^0 bending band at 650 cm^{-1}.

Systematic changes of vibrational frequencies and intensity ratios of important bands occur as a result of dissolved CO_2 in quenched Sm melt (Figs. 7 and 8; Table 5). The spectroscopic features near 500 cm^{-1} remain unaltered with addition of CO_2. In view of the discussion above, this observation is interpreted to mean that three-dimensional structural units occur in CO_2-bearing Sm melts with the CO_2 contents used here (Table 1). The band near 650 cm^{-1} also remains as CO_2 is added except in the two most CO_2-rich samples (5.9 and 5.2 wt. percent CO_2; Table 1), which indicates that chain units also remain in the CO_2-bearing melt. The data do indicate, however, that the proportion of such units may have decreased as CO_2 is dissolved in the melt.

In the high-frequency envelope (Figs. 7 and 8), generally there are at least three bands in addition to the C–O stretch band near 1070 cm^{-1}. The strongest band is near 1000 cm^{-1} and probably corresponds to an Al-bearing structural unit with NBO/T near 1 (sheet). In addition, there is a medium to strong band near 930–940 cm^{-1} and a very weak band near 860 cm^{-1}. In view of the diminished intensity of the 650 cm^{-1} band with the addition of CO_2 to the melt, we suggest that the 860 cm^{-1} band is the associated stretch band (chain). Its lower frequency compared with the CO_2-free melt may indicate lower Si/(Si + Al) of this structural unit. Its lower intensity relative to the other bands in the high-frequency envelope indicates lower abundance.

The remaining band in the high-frequency envelope may be the stretch band associated with the occurrence of aluminous, three-dimensional structural units in the melt. The other evidence for such units is the band near 500 cm^{-1}. The 500 cm^{-1} band frequency corresponds to that of the rocking band in three-dimensional aluminosilicate melts such as those of $NaAlSiO_4$ and $CaAl_2Si_2O_8$ composition. The frequencies of the Si(Al) coupled stretch bands are also similar (Virgo *et al.*, 1979). The lower frequency of this band compared with its position in CO_2-free Sm melt indicates a decrease in Si/(Si + Al). Its

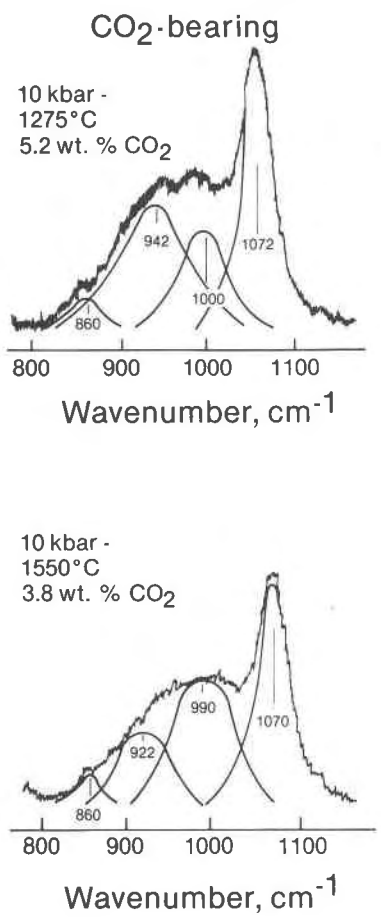

Fig. 8. High-frequency envelope of CO_2-bearing Sm quenched melt. (Ar^+ laser, 200–400 mW power.)

greater intensity relative to the other bands in the high-frequency envelope compared with the CO_2-free samples (Figs. 7 and 8) indicates that the abundance of three-dimensional structural units in the melt has increased as the result of dissolved CO_2.

Solubility mechanisms

$CaMgSi_2O_6 + CO_2$

According to our data, solution of CO_2 in Di melts to form carbonate complexes is accompanied by a reduction of isolated SiO_4^{4-} tetrahedra relative to chain and sheet units in the melt. There are no indications that new silicate units have been formed with the amounts of CO_2 added to these experiments (see Table 1).

Inasmuch as the CO_2 solubility is positively correlated with Ca/(Ca + Mg) in meta- and orthosilicate melts (Holloway *et al.*, 1976), it appears that the CO_3^{2-} anion is closely associated with Ca^{2+} in the melt by formation of $CaCO_3$. The increasing degree of polymerization of the melt with increasing carbonate content is in response to the formation of such complexes. The CO_2 solubility is controlled primarily by the activity of Ca^{2+}, and not by the degree of polymerization of the melt as suggested by Holloway *et al.* (1976).

Eggler and Rosenhauer (1978) surveyed the data on the influence of CO_2 on silicate phase equilibria and its solubility in silicate melts. They concluded that in melts that contain nonbridging oxygens, the principle of the solubility mechanism may be illustrated with the expression:

$$CO_2(gas) + 2O^-(NBO) = CO_3^{2-}\ (melt) + O^0\ (BO) \quad (4)$$

This mechanism is consistent with our conclusions. The nonbridging oxygen (NBO) to form bridging oxygen (BO) may be derived from $Si_2O_6^{4-}$ or $Si_2O_5^{2-}$ units or both:

$$2SiO_4^{4-}\ (melt) + 2CO_2(gas) = Si_2O_6^{4-}\ (melt) + 2CO_3^{2-}\ (melt) \quad (5)$$

and

$$2SiO_4^{4-}\ (melt) + 3CO_2\ (gas) = Si_2O_5^{2-}\ (melt) + 3CO_3^{2-}\ (melt) \quad (6)$$

Chains could also be transformed to sheets:

$$Si_2O_6^{4-}\ (melt) + CO_2\ (gas) = Si_2O_5^{2-}\ (melt) + 2CO_3^{2-}\ (melt) \quad (7)$$

The spectroscopic data cannot be used to determine whether sheets are formed at the expense of chains, or whether equations 4 or 5 represent the most accurate description of the interaction between the anionic network of the melt and CO_2 in solution in the melt. Note, however, that Dent Glasser (1979), in a review of crystal structures of silicates, concluded, on the basis of charge density considerations relating to modifying cations that $Si_2O_5^{2-}$ (sheet) structures are less stable than $Si_2O_6^{4-}$ (chain) structures when balanced with alkaline earth cations. In fact, alkaline earth sheet structures do not occur in a crystallized form. We suggest, therefore, that equation 5 probably describes the interaction between the melt and CO_2 most accurately. This equation may then be combined with equation 2 to describe the solubility mechanism in metasilicate melts such as those of Di composition:

$$5Si_2O_6^{4-}\ (melt) + 2\ CO_2\ (gas) = 2SiO_4^{4-}\ (melt) + 4Si_2O_5^{2-}\ (melt) + 2CO_3^{2-}\ (melt) \quad (8)$$

$NaCaAlSi_2O_7 + CO_2$

The influence of dissolved CO_2 on the anionic complexes in Sm melt is less well defined than in Di melt, partly because Sm melt is a combination of more polymerized units such as three-dimensional network, sheets, and chains, whereas Di melt also has a large proportion of orthosilicate and little or no three-dimensional network component. As a result, Raman spectra are less sensitive to the changes of Sm melt structure than of Di melt structure.

The Raman data (Figs. 7 and 8; Table 5) indicate that the formation of CO_3^{2-} complexes in the melt results in polymerization of the silicate network, as the proportion of three-dimensional structural units has increased substantially relative to chain and sheet units.

The principles governing the solubility of CO_2 in Sm melt are, therefore, similar to those for CO_2 in Di melt. The main difference is that the expression that illustrates the interaction between CO_2 and the silicate network must take into account the different structural units in the two melts.

There are two reasons why $(CaCO_3)^0$ rather than $(Na_2CO_3)^0$ type complexes probably are formed in Sm melt. First, as also summarized above, solubility studies of CO_2 in silicate melts always indicate that carbonate complexes are associated with Ca^{2+} cations rather than other monovalent or divalent cations in the melt. Second, as suggested by Bottinga and Weill (1972) and also pointed out by Virgo *et al.* (1980), MAl^{4+} complexes are more stable than $M_{0.5}Al^{4+}$ complexes.

Inasmuch as three-dimensional structural units appear to become more abundant as CO_2 is dissolved in Sm melt, the solubility mechanism may now be illustrated with the equation:

$$T_2O_6^{4-}\text{ (melt)} + 2CO_2\text{ (gas)} = 2TO_2\text{ (melt)} + 2CO_3^{2-}\text{ (melt)} \quad (9)$$

Equation 9 may be combined with equation 3 to give the complete reaction:

$$4T_2O_5^{2-}\text{ (melt)} + 2CO_2\text{ (gas)} = T_2O_6^{4-}\text{(melt)} + 6TO_2\text{ (melt)} + 2CO_3^{2-}\text{ (melt)} \quad (10)$$

where $T = Si^{4+} + (NaAl)^{4+}$ and the carbonate is associated with Ca^{2+}.

Applications

Most phase-equilibrium studies of the role of CO_2 in the formation and evolution of magma at high pressures and temperatures have been conducted in systems that do not contain amphoteric oxides. These studies (Eggler, 1973, 1974, 1975, 1976, 1978; Eggler and Rosenhauer, 1978, Huang and Wyllie, 1976) have shown that the addition of CO_2 results in the liquidus boundary between two minerals of different degree of polymerization (*e.g.*, forsterite and enstatite) shifting toward the silica-deficient portion of the systems. The solubility mechanism of CO_2 in simple silicate melts without amphoteric oxides also indicates that more polymerized minerals would precipitate from the CO_2-saturated silicate melts, because the concentration of more polymerized species in the melt increases with increasing CO_2 content.

Even though the Di composition is useful to demonstrate the solubility mechanism of CO_2 in silicate melts that contain nonbridging oxygens, this composition is a gross oversimplification of natural magma. The greatest difference is the absence of amphoteric oxides such as Al_2O_3 and Fe_2O_3. The Sm composition contains 19.74 wt. percent Al_2O_3 and about 46 wt. percent SiO_2. Basaltic rocks usually contain about 18–21 wt. percent total amphoteric oxides (Chayes, 1975). Consequently, with the assumption that the structural roles of Al^{3+} and Fe^{3+} are similar in basaltic magma, the Sm composition represents a closer approximation of the natural magma. Our data indicate that the solubility mechanism of CO_2 in simple binary silicate melts resembles that of the more complex Sm composition. We conclude, therefore, that the data acquired in such simple systems provide an accurate basis on which to provide information on the influence of CO_2 on natural basaltic magma.

Acknowledgments

Critical reviews by G. E. Brown, S. A. Brawer, J. R. Holloway, W. Harrison, F. J. Ryerson, and H. S. Yoder, Jr. are appreciated. This research was partially supported by NSF grant EAR 7911313 and partially by the Carnegie Institution of Washington.

References

Bates, J. B., R. W. Hendricks and L. B. Shaffer (1974) Neutron irradiation effects and structure of non-crystalline SiO_2. *J. Chem. Phys., 61,* 4163–4176.

Bottinga, Y. and D. F. Weill (1972) The viscosity of magmatic silicate liquids: a model for calculation. *Am. J. Sci., 272,* 438–475.

Boyd, F. R. and J. L. England (1960) Apparatus for equilibrium measurements at pressures up to 50 kilobars and temperatures up to 1750°C. *J. Geophys. Res., 65,* 741–748.

——— and ——— (1963) Effect of pressure on the melting of diopside, $CaMgSi_2O_6$, and albite, $NaAlSi_3O_8$, in the range up to 50 kb. *J. Geophys. Res., 68,* 311–323.

Brawer, S. A. (1975) Theory of the vibrational spectra of some network and molecular glasses. *Phys. Rev. B, 11,* 3173–3194.

——— and W. B. White (1975) Raman spectroscopic investigation of the structure of silicate glasses. I. The binary silicate glasses. *J. Chem. Phys., 63,* 2421–2432.

——— and ——— (1977) Raman spectroscopic investigation of the structure of silicate glasses. II. Soda-alkali earth-alumina ternary and quaternary glasses. *J. Non-Cryst. Solids, 23,* 261–278.

Brey, G. P. and D. H. Green (1976) Solubility of CO_2 in olivine melilitite at high pressure and the role of CO_2 in the earth's upper mantle. *Contrib. Mineral. Petrol., 55,* 217–230.

Chayes, F. (1975) Average composition of the commoner Cenozoic volcanic rocks. *Carnegie Inst. Wash. Year Book, 75,* 547–549.

Delaney, J. R., W. W. Muenow and D. G. Graham (1978) Abundance and distribution of water, carbon and sulfur in the glassy rims of submarine pillow basalts. *Geochim. Cosmochim. Acta, 42,* 581–594.

Dent Glasser, L. S. (1979) Non-existent silicates. *Z. Kristallogr., 149,* 291–305.

Eggler, D. H. (1973) Role of CO_2 in melting processes in the mantle. *Carnegie Inst. Wash. Year Book, 72,* 457–467.

——— (1974) Application of a portion of the system $CaAl_2Si_2O_8$–$NaAlSi_3O_8$–SiO_2–MgO–Fe–O_2–H_2O–CO_2 to genesis of the calc-alkaline suite. *Am. J. Sci., 274,* 297–315.

——— (1975) Peridotite–carbonatite relations in the system CaO–MgO–SiO_2–CO_2. *Carnegie Inst. Wash. Year Book, 74,* 468–474.

——— (1976) Does CO_2 cause partial melting in the low-velocity layer of the mantle? *Geology, 2,* 69–72.

——— (1978) The effect of CO_2 upon partial melting in the system Na_2O–CaO–Al_2O_3–MgO–SiO_2–CO_2 to 35 kb, with an analysis of melting in a peridotite–H_2O–CO_2 system. *Am. J. Sci., 278,* 305–343.

——— and M. Rosenhauer (1978) Carbon dioxide in silicate melts. II. Solubility of CO_2 and H_2O in $CaMgSi_2O_6$ (diopside) liquids and vapors at pressures to 40 kb. *Am. J. Sci., 278,* 64–94.

———, B. O. Mysen and T. C. Hoering (1974) Gas species in sealed capsules in solid-media, high-pressure apparatus. *Carnegie Inst. Wash. Year Book, 73,* 228–232.

———, J. R. Holloway and T. C. Hoering (1979) The solubility of carbon monoxide in silicate melts at high pressures and its effect on silicate phase relations. *Earth Planet. Sci. Lett., 43,* 321–330.

Etchepare, J. (1972) Study by Raman spectroscopy of crystalline and glassy diopside. In R. W. Douglas and B. Ellis, Eds., *Amorphous Materials,* p. 337–346. Wiley, New York.

Furukawa, T. and W. B. White (1980) Raman spectroscopic investigation of the structure of silicate glasses. III. Alkali–silico–germanates. *J. Chem. Phys.,* in press.

———, S. A. Brawer and W. B. White (1978) The structure of lead silicate glasses determined by vibrational spectroscopy. *J. Mater. Sci., 13,* 268–282.

Gerlach, T. M. and G. E. Nordlie (1975) The C–O–H–S system. Part I. Compositional limits and trends in basaltic glasses. *Am. J. Sci., 275,* 353–376.

Green, H. W., II (1972) A CO_2 charged asthenosphere. *Nature, 238,* 2–5.

Holloway, J. R., B. O. Mysen and D. H. Eggler (1976) The solubility of CO_2 in liquids on the join CaO–MgO–SiO_2–CO_2. *Carnegie Inst. Wash. Year Book, 75,* 626–631.

Huang, W. L. and P. J. Wyllie (1976) Melting relationships in the systems CaO–CO_2 and MgO–CO_2 to 33 kilobars. *Geochim. Cosmochim. Acta, 40,* 129–132.

Irving, A. J. and P. J. Wyllie (1975) Subsolidus and melting relationships for calcite, magnesite on the join $CaCO_3$–$MgCO_3$ to 36 kb. *Geochim. Cosmochim. Acta, 39,* 35–53.

Kadik, A. A. and D. H. Eggler (1975) Melt–vapor relations on the join $NaAlSi_3O_8$–H_2O–CO_2. *Carnegie Inst. Wash. Year Book, 74,* 479–484.

Lazarev, A. N. (1972) *Vibrational spectra and structure of silicates.* Consultants Bureau, New York.

Lentz, C. W. (1964) Silicate minerals as sources of trimethylsilyl silicates and silicate structure analysis of sodium silicate solutions. *Inorg. Chem., 3,* 574–579.

Mao, H. K., P. M. Bell and J. L. England (1971) Tensional errors and drift of thermocouple electromotive force in the single-stage, piston–cylinder apparatus. *Carnegie Inst. Wash. Year Book, 70,* 281–287.

Masson, C. R. (1968) Ionic equilibria in liquid silicates. *J. Am. Ceram. Soc., 51,* 134–143.

McGetchin, T. R. and J. R. Besancon (1973) Carbonate inclusions in mantle-derived pyropes. *Earth Planet. Sci. Lett., 18,* 408–410.

Mysen, B. O. (1976) The role of volatiles in silicate melts: solubility of carbon dioxide and water in feldspar, pyroxene and feldspathoid melts to 30 kb and 1626°C. *Am. J. Sci., 276,* 969–996.

——— and M. G. Seitz (1975) Trace element partitioning determined by beta-track mapping—an experimental study using carbon and samarium as examples. *J. Geophys. Res., 80,* 2627–2635.

———, D. H. Eggler, M. G. Seitz and J. R. Holloway (1976) Carbon dioxide in silicate melts and crystals. I. Solubility measurements. *Am. J. Sci., 276,* 455–479.

Presnall, D. C., N. L. Brenner and T. H. O'Donnell (1973) Thermocouple drift of PtPt10Rh and W3Re/W25Re thermocouples in single stage piston–cylinder apparatus. *Am. Minerals., 58,* 771–777.

Roedder, E. (1965) Liquid CO_2 inclusions in olivine-bearing nodules and phenocrysts from basalts. *Am. Mineral., 50,* 1746–1782.

Sharma, S. K. (1979) Structure and solubility of carbon dioxide in silicate glasses of diopside and sodium melilite compositions at high pressures from Raman spectroscopic data. *Carnegie Inst. Wash. Year Book, 78,* 532–537.

Smart, R. M. and F. P. Glasser (1978) Silicate anion constitution of lead silicate glasses and crystals. *Phys. Chem. Glasses, 19,* 95–102.

Taylor, M. and G. E. Brown (1979) Structure of mineral glasses. I. The feldspar glasses $NaAlSi_3O_8$, $KAlSi_3O_8$, $CaAl_2Si_2O_8$. *Geochim. Cosmochim. Acta, 43,* 61–77.

Verweij, H. (1979a) Raman study of the structure of alkali germanosilicate glasses. I. Sodium and potassium metasilicate glasses. *J. Non-Cryst. Solids, 33,* 41–53.

——— (1979b) Raman study of the structure of alkali germanosilicate glasses. II. Lithium, sodium and potassium digermanosilicate glasses. *J. Non-Cryst. Solids, 33,* 55–69.

——— and W. L. Konijnendijk (1976) Structural units in K_2O–PbO–SiO_2 glasses by Raman spectroscopy. *J. Am. Ceram. Soc., 59,* 517–521.

———, H. Van Den Boom and R. E. Breemer (1977) Raman scattering of carbonate ions dissolved in potassium silicate glasses. *J. Am. Ceram. Soc., 60,* 529–534.

Virgo, D., B. O. Mysen and I. Kushiro (1980) Anionic constitution of silicate melts quenched at 1 atm from Raman spectroscopy: implications for the structure of igneous melts. *Science,* in press.

———, F. Seifert and B. O. Mysen (1979) Three-dimensional network structures of melts in the systems $CaAl_2O_4$–SiO_2, $NaAlO_2$–SiO_2, $NaFeO_2$–SiO_2, and $NaGaO_2$–SiO_2 at 1 atm. *Carnegie Inst. Wash. Year Book, 78,* 506–511.

White, W. B. (1974) The carbonate minerals. In V. C. Farmer, Ed., *The Infrared Spectra of Minerals,* p. 227–284. Mineralogical Society, London.

Wyllie, P. J. and W.-L. Huang (1976) Carbonation and melting reactions in the system CaO–MgO–SiO_2–CO_2 at mantle pressures with geophysical and petrological applications. *Contrib. Mineral. Petrol., 54,* 79–104.

Manuscript received, October 1, 1979;
accepted for publication, June 2, 1980.